Materials Advances

ROYAL SOCIETY OF CHEMISTRY

PAPER

View Article Online
View Journal | View Issue

Cite this: *Mater. Adv.*, 2025, **6**, 1497

Synthesis and preclinical evaluation of novel L-cystine-based polyamide nanocapsules loaded with a fixed-dose combination of thymoquinone and doxorubicin for targeted pulmonary anticancer drug delivery

Hadeel Fayez Banat,[a] Dalia Khalil Ali,[b] Qais Jarrar,[a] Esra'a Alomary[a] and Eman Zmaily Dahmash *[ac]

Innovative synthetic biodegradable polymers containing amino acid moieties are used as pulmonary anticancer drug delivery systems to efficiently administer drugs in a controlled manner while also altering the physical and chemical characteristics of therapeutic molecules and the way they are delivered to the lungs. In this study, the aim was to prepare a new polyamide based on L-cystine amino acid loaded with a combination of thymoquinone (TQ) and doxorubicin (DOX) nanocapsules (TQ-DOX/Cys-Py/PA NCs) to be delivered directly to the lungs. TQ-DOX/Cys-Py/PA NCs were created using a single-step interfacial polycondensation method. The aerodynamic performance assessment shows that the prepared TQ-DOX/Cys-Py/PA NCs were able to deliver 98.7% and 97.1% of the TQ and DOX nominated dose, respectively. TQ and DOX with emitted doses of 2008.2 and 110.2 μg can reach the lower parts of the respiratory system and have an aerodynamic particle size between 1 and 5 μm, which revealed that the optimum formulation would produce a small particle size (19.89 nm) with high entrapment efficiency (TQ: 85.4%, DOX: 99.49%) and loading efficiency (TQ: 52.2%, DOX: 15.03). The targeted release of TQ and DOX in 0.1 M GSH-containing buffer solution demonstrated a faster onset of action, with 50% released within the first 2 hours. *In vivo* studies were conducted to demonstrate the efficacy of TQ-DOX/Cys-Py/PA NCs in enabling targeted drug delivery to the lungs for the treatment of lung cancer. The results demonstrate exceptional lung targeting and sustained lung retention for at least 24 hours. Furthermore, the toxicity of the TQ-DOX/Cys-Py/PA NCs was assessed by quantifying the protein carbonyl content. The results showed that the TQ-DOX/Cys-Py/PA NCs exhibited reduced toxicity to the heart, liver, and kidney compared to free DOX and DOX/Cys-Py/PA NCs.

Received 26th September 2024,
Accepted 20th January 2025

DOI: 10.1039/d4ma00972j

rsc.li/materials-advances

1. Introduction

Development of novel polymer-based drug delivery systems is required to effectively deliver drugs in a regulated manner while also modifying the physicochemical and pharmacokinetic properties of therapeutic molecules.[1–5] Polymer nanotechnology focuses on reducing the toxicity of anticancer drugs and improving their bioavailability.[6–8]

Pulmonary drug delivery is a favourable alternative method of administering drugs, offering numerous advantages compared to conventional routes.[9,10] It involves minimal enzymatic exposure, has fewer systemic side effects, avoids the first-pass metabolism impact and delivers a higher and more concentrated amount of medication to the site of the disease.[11,12] Pulmonary drug delivery allows for direct drug access to the lungs with minimal side effects and a rapid pharmacological response and is considered a promising alternative strategy for the treatment of lung cancer.[13,14] Pulmonary drug delivery formulations can be composed of either the drug alone or the drug combined with a compatible carrier. Different types of carriers, including lipids, sugars, and polymers, are utilized for transporting pulmonary drugs to the lungs.[15–19]

Amino acids are precious building blocks that can be used to design biodegradable or biocompatible polyamides with many

[a] *Department of Applied Pharmaceutical Sciences and Clinical Pharmacy, Faculty of Pharmacy, Isra University, Amman, Jordan*
[b] *Department of Physiotherapy Department, Faculty of Allied Medical Sciences, Isra University, Amman, Jordan*
[c] *Department of Chemical and Pharmaceutical Sciences, School of Life Sciences, Pharmacy and Chemistry, Kingston University London, Kingston Upon Thames KT1 2EE, London, UK. E-mail: eman.dahmash@kingston.ac.uk*

physical features.[20–22] Creating novel synthetic biodegradable polymers with amino acid moieties for use as drug delivery systems is highly desirable.[23,24] Among the several categories of polymers, polyamides prepared using amino acids possess notable characteristics like excellent biocompatibility, gradual degradability, and versatile physicochemical modification capabilities.[25,26] The hydrophilicity of the constituent amino acids in the polymer affects the degradation rates of the polymer chain.[27–29] Polyamides are employed in the composition of chemotherapeutics to achieve targeted administration over a specific period, thereby reducing drug-related side effects and enhancing effectiveness.[30,31]

A targeted drug delivery system utilising cystine amino acid as a diamine monomer to create a nonpeptidic polyamide with a biodegradable component due to the reduction of disulfide bonds would be appealing. Polymers with disulfide bonds can react with the elevated levels of glutathione inside cells and release the drugs they carry by undergoing disulfide–thiol exchange reactions with GSH. These polyamides were used to regulate the release of anticancer medications due to the increased concentration of GSH in some tumour cells compared to normal cells.[32–35]

Doxorubicin (DOX) is a highly effective drug for the treatment of various hematopoietic malignancies and solid tumours. Its use has been limited because of the low bioavailability and severe side effects, such as irreversible cardiotoxicity, ROS production, targeting topoisomerase IIβ in cardiomyocytes, DNA damage, therapy-related malignancy, and gonadotoxicity.[36,37] Due to these limitations, new formulations containing DOX have been developed.[38–42]

Thymoquinone (TQ) is obtained from the black seed, a plant that has shown effectiveness in the treatment of cancer. Studies have shown that the effectiveness of the treatment is improved when it is enclosed in a liposome that is specifically designed to target cancer cells. Multiple studies have demonstrated that TQ possesses the capacity to impede the progression of the tumour cell cycle. Pharmacokinetic studies have demonstrated that TQ exhibits a low bioavailability, a sluggish absorption rate, and a rapid elimination rate.[43–45]

Co-administering TQ with other chemotherapeutic drugs can synergistically enhance their therapeutic efficacy while minimising their toxic effects on cells.[46] The combination of anticancer drugs TQ and DOX can minimise cytotoxicity and simultaneously maximise efficacy. Encapsulated TQ into lipid-polymer nanoparticles was reported to enhance its anticancer and oral delivery efficiency. TQ nanoparticles with free DOX were prepared to increase DOX efficiency.[47] The results demonstrate that the co-delivery of encapsulated TQ through oral administration and free DOX could improve the anticancer efficiency of DOX and result in a higher anticancer activity of the encapsulated TQ nanoparticles than free TQ. In addition, this delivery system enhances the TQ bioavailability and cellular uptake.[48–50]

Several independent studies have indicated that combining TQ and DOX anticancer drugs can have a substantial effect, reducing the harmful effects on cells while maximising effectiveness. However, the potential of using polymeric nanocapsules derived from cystine amino acid to enhance the delivery of TQ with DOX for lung cancer treatment remains unexplored. These newly synthesized TQ–DOX polyamide based nanocapsules could serve as a promising drug delivery system, potentially revolutionising lung cancer treatment. We hypothesise that pulmonary drug administration of these polymeric nanocapsules of anticancer drugs TQ and DOX could directly target the lungs, bypassing cytotoxicity and offering a new ray of hope in the fight against lung cancer.[51–55]

2. Materials and methods

2.1 Materials

L-Cystine amino acid, DOX and TQ were purchased from Sigma Chemicals Co. (Pool, UK). Chloroform, acetonitrile, trifluoroacetic acid (TFA), HPLC grade water (H_2O), dimethylsulphoxide (DMSO), dimethylformamide (DMF), dithiothreitol (DTT) and phosphate buffered saline (PBS) were supplied by Alpha Chemika (Mumbai, India). Methanol and thionyl chloride were supplied by Tedia high-purity solvents (Fairfield, USA). 2,6-Pyridinedicarbonyl dichloride was obtained from Thermo Fisher Scientific (Karlsruhe, Germany). The protein carbonyl content kit was obtained from Abcam (Cambridge, United Kingdom).

2.2 Polyamide and TQ–DOX loaded polyamide

2.2.1 Synthesis of L-cystine based polyamide (Cys-Py/PA). A mixture of L-cystine (1.20 g, 5 mmol) and NaOH (0.40 g, 10 mmol) was dissolved in 15 mL of distilled water in a 100 mL round bottom flask. The reaction mixture was cooled in an ice bath with vigorous stirring. A solution of 2,6-pyridinedicarbonyl dichloride (1.02 g, 5 mmol) dissolved in 10 mL of chloroform was then added to the cystine aqueous reaction mixture and stirred for 30 minutes. Cys-Py/PA was filtered using suction filtration with filter papers having pore sizes as small as 0.1 μm, then washed with distilled water and acetone, and then dried in a freeze-dryer for 24 hours to remove the residual solvent.

2.2.2 Synthesis of L-cystine based polyamide loaded with TQ and DOX nanocapsules (TQ-DOX/Cys-Py/PA NCs). A mixture of L-cystine (1.20 g, 5 mmol), NaOH (0.40 g, 10 mmol), and DOX (25 mg) was dissolved in 15 mL of distilled water in a 100 mL round bottom flask. The reaction mixture was cooled in an ice bath with vigorous stirring. A solution containing 2,6-pyridinedicarbonyl dichloride (1.02 g, 5 mmol) and TQ (200 mg) dissolved in 10 mL of chloroform was then added to the cystine aqueous solution and stirred for 30 minutes. The TQ-DOX/Cys-Py/PA nanocapsules were filtered using suction filtration with filter papers having pore sizes as small as 0.1 μm and washed with distilled water and then dried in a freeze-dryer for 24 hours to remove the residual solvent. Other formulas were also investigated, the one with 25 mg of DOX (DOX/Cys-Py/PA) NCs and the other with 200 mg of TQ (TQ/Cys-Py/PA) NCs.

2.3 High performance liquid chromatography (HPLC) for the quantification of TQ and DOX

The Dionex Ultimate 3000 HPLC was used for concurrent quantitative analysis of TQ and DOX, and an appropriate method was developed for each drug. The provided system uses a gradient pump, UV detector set at 250 nm (TQ) and 550 nm (DOX), and Fortis C18 analytical column (Fortis Technologies Ltd C18, 250 × 4.6 mm). The mobile phase consisted of acetonitrile:0.1% TFA in water (85 : 15 v/v). The temperature of the sample was set at 27 °C. The sample injection volume was 10 μL with a flow rate of 0.8 mL min^{-1}. The run time was 12 minutes. In terms of specificity, accuracy, precision, and linearity, as well as limits of detection and quantification, the HPLC technique was validated according to ICH guidelines.[56] For the calibration curve, samples were prepared in acetonitrile and serial dilutions were made using the same solvent.

2.4 Characterisation of the polyamide and TQ-DOX loaded polyamides

2.4.1 Solubility test. The solubility test was performed by dissolving 10 mg of Cys-Py/PA and TQ-DOX/Cys-Py/PA NCs in 5 mL of various solvents (water, methanol, ethanol, chloroform, acetone, diethyl ether, DMSO, DFA, and acetonitrile) at 25 °C. Then the apparent solubility was visually evaluated.

2.4.2 Entrapment efficiency (EE) and drug loading capacity (DLC). After filtration of the prepared nanoparticles, 10 microliters of a known volume filtrate were injected into the HPLC equipment to calculate the EE% for TQ and DOX in the TQ-DOX/Cys-Py/PA NCs using eqn (1).

$$\text{EE } (\%) = \frac{\text{Drug}_t - \text{Drug}_f}{\text{Drug}_t} \times 100 \quad (1)$$

where Drug_t is the total amount of TQ or DOX that was added to the formula and Drug_f is the total amount of TQ or DOX that were present in the filtrate and were not encapsulated during the polymerisation process.

As for DLC, 10 mg of TQ-DOX/Cys-Py/PA NCs was dissolved in 10 mL of DMSO and 10 μL were injected into an HPLC using the same method to calculate the DLC% of TQ and DOX in TQ-DOX/Cys-Py/PA NCs. The DLC was determined using eqn (2).

$$\text{DLC } (\%) = \frac{\text{Weight of the drug in NCs}}{\text{Weight of the NCs}} \times 100 \quad (2)$$

2.4.3 Fourier transform infrared (FTIR) spectroscopy analysis. A PerkinElmer FTIR spectrometer (OH, USA) was utilised to record FTIR spectra of the polymer using Spectrum 10 software. The test was done by putting a few milligrams of the sample into the sample holder above a laser lens and secured with an appropriate adapter. The FTIR spectral scans for each sample were performed using attenuated FTIR spectroscopy with a resolution of 2 cm^{-1} spanning the range of 450–4000 cm^{-1}.

2.4.4 Nuclear magnetic resonance (NMR) spectroscopy analysis. For the ^{1}H-NMR and ^{13}C-NMR measurements, tetramethylsilane (TMS) was used as an internal standard. The ^{1}H NMR was carried out at 500 MHz while the ^{13}C NMR was conducted at 125 MHz to analyse the polymer using a Bruker Avance DPX NMR spectrometer (Bruker DPX-500) from Massachusetts, USA.

2.4.5 Transmission electron microscopy (TEM). The TEM image of Cys-Pyr PA was captured using an FEI Morgagni 268D TEM (Hillsboro, OR, USA). The process involved preparing a suspension of the sample (around 0.05 mg mL^{-1}) using deionised water as a suspending medium. Then, about 10 μL of the prepared suspension was placed on a copper grid and left for a few minutes to allow the nanoparticles to settle on the grid. Then, the excess solvent was removed using filter paper and the sample was placed in a TEM for imaging. Images were then processed using Image J software (Fiji).

2.4.6 Differential scanning calorimetry (DSC) analysis. The DSC analysis of the TQ, DOX, Cys-Py/PA, and TQ-DOX/Cys-Py/PA NCs was carried out using a DSC 25-TA instrument (DSC25, TA instruments Trios V5.6.0.75). About 3–5 mg of the sample was placed in an aluminium pan and subjected to heating at a rate of 10 °C min^{-1} using nitrogen gas at a flow rate of 50 mL min^{-1}. Scans were run from 25 to 300 °C.

2.4.7 Thermogravimetric analysis (TGA). The thermal stability of the polymer alone and with the added active ingredients was investigated using TGA. Samples (a few milligrams) of Cys-Py/PA and TQ-DOX/Cys-Py/PA NCs were analysed using TGA, where the samples were loaded into TGA pans and analysed under a nitrogen atmosphere using a TGA instrument (TGA550, TA instruments Trios V5.6.0.75). The analysis involved monitoring weight changes while heating from 25 to 400 °C at a heating rate of 10 °C min^{-1}.

2.4.8 Analysis of the particle size, polydispersity index (PDI), and zeta potential. The mean hydrodynamic diameter, PDI, and zeta potential of TQ, DOX, Cys-Py/PA, TQ/Cys-Py/PA NCs, DOX/Cys-Py/PA NCs and TQ-DOX/Cys-Py/PA NCs were determined at 25 °C using a Zetasizer Nano ZS90 instrument, Malvern Instruments (Worcestershire, UK). Before the analysis, a few milligrams of the samples were diluted with deionised water and subjected to sonication for 30 seconds at medium amplitude (60 Hz) without heat to break aggregates. The analysis was conducted in triplicate, and the results were presented as mean ± standard deviation (SD).

2.4.9 X-ray diffraction (XRD) analysis. The XRD analysis was performed to investigate the crystalline nature and structural properties of Cys-Py/PA and TQ-DOX/Cys-Py/PA NCs. The experiments were conducted using a Bruker-AXS D8 X-ray diffractometer (Sheffield, UK). The samples were placed in the instrument's sample holder, and X-ray scans were conducted over a specified range of diffraction angles (from 5° to 60° 2-Theta). The obtained diffraction patterns were analysed to identify the crystallinity of the samples.

2.5 *In vitro* study

2.5.1 *In vitro* aerodynamic aerosolization of the TQ-DOX/Cys-Py/PA NCs. The next-generation impactor NGI (Copley Scientific Limited Model 170, UK) was used to assess the *in vitro* deposition of TQ and DOX and the aerodynamic particle size distribution. Setting the pump flow rate to 60 L min^{-1}

resulted in a flow rate of 4 litres for almost four seconds. Six capsules manually filled with 14 mg of the TQ-DOX/Cys-Py/PA NCs and placed in an Aerolizer® device were used to assess TQ and DOX aerosolisation performance. The formula used in each capsule is expected to contain 2 mg and 7 mg of DOX and TQ respectively. Each test included six capsules to ensure accurate quantification of the APIs. After the actuation of the six capsules, the device was opened, and TQ and DOX content in each tray was obtained by dissolving the content of each tray in 10 mL of DMSO. The trays were then placed in the sonication bath set at medium altitude without heating for 10 minutes to aid the dissolution of the two drugs. After that, the liquid in the 8 trays, as well as the pre-separator, and the induction tube were transferred into a volumetric flask, and the volume was adjusted with DMSO. Samples were filtered using syringe membrane filters (0.45 μm) and then analysed using the validated HPLC method.

The results obtained from the NGI analysis were used to calculate the main aerodynamic performance parameters of the formula. The cumulative quantity of TQ or DOX collected from the induction tube, the pre-separator, trays 1–7 and the final micro-orifice collector (MOC) were used to calculate the emitted dose (ED%), as can be seen from eqn (3). ED is a true representation of the efficiency of the formulation to be discharged from the capsules. The next parameter is the respirable dosage (RD), which is the representation of the total amount of the formula that can reach the lower parts of the respiratory system, which is within the size range of 1–5 μm and is the sum of drug content from trays 2 to 7. The last aerodynamic parameters are the fine particle fraction of the emitted dose (FPF_{ED}) and the fine particle fraction of the theoretical dose (FPF_{TD}). These two parameters were calculated using eqn (4) and (5) respectively.

$$\text{ED}\ (\%) = \frac{\text{Cumulative drug content}}{\text{Theoretical drug content}} \times 100 \quad (3)$$

$$\text{FPF}_{\text{ED}}\ (\%) = \frac{\text{RD}}{\text{ED}} \times 100 \quad (4)$$

$$\text{FPF}_{\text{TD}}\ (\%) = \frac{\text{RD}}{\text{TD}} \times 100 \quad (5)$$

2.5.2 Release study. The release of TQ and DOX from the TQ-DOX/Cys-Py/PA NCs was investigated using the dialysis membrane method, which is described in the literature.[57] 10 mg of the TQ-DOX/Cys-Py/PA NCs was weighed and redispersed in 5 mL of PBS (pH 7.4). The release of DOX and TQ (TQ-DOX/Cys-Py/PA) nanocapsules at pH 7.4, the condition that mimics the lung environment, facilitates the identification of the optimal physicochemical properties. They were then placed in dialysis bags (Sigma-Aldrich, Pool, UK) [molecular weight cut-off of 14 000–16 000 Da]. The bags were suspended in 30 mL of PBS in beakers and kept in a shaking water bath at 37 °C and 100 rpm covered. 1 mL was withdrawn from the beaker at 0.5, 1, 2, 3, 4, 5, 6, 7, 8, 9, 10, 12, 14, 16, 20 and 24 h. The TQ and DOX API content was quantified using the validated HPLC method. Fresh PBS was added after each withdrawal to maintain the sink conditions. Another 10 mg of the TQ-DOX/Cys-Py/PA NCs was also prepared and was dispersed in PBS that contained 0.1 M glutathione (GSH) and the same procedure was carried out. The experiment was performed in triplicate and results were calculated as mean % release ±SD.

2.6 *In vivo* studies

2.6.1 Animal husbandry. In this experiment, 72 Swiss albino male mice were used with an average weight of 25–30 g. The mice were kept in a well-ventilated room under suitable and controlled environmental conditions (22–25 °C, 67–77% humidity, and 12/12-hour dark/light cycle). The animal handling procedures followed the Institutional Animal Care and Use Committee guidelines. The Scientific Research Ethics Committee approved the animal use of Isra University (4-18/2022/2023).

2.6.2 *In vivo* aerodynamic distribution study. In this study, 48 male mice were randomly divided into eight groups (n = 6 mice per group) and treated with 17 mg of the inhaled (TQ-DOX/Cys-Py/PA) NCs containing 2.5 mg of DOX and 9 mg of TQ using a dry powder insufflator.[57] Each mouse of each group was exposed to 3 puffs of TQ-DOX/Cys-Py/PA NCs using the dry powder insufflator, and the mice were sacrificed at 0, 0.5, 1, 2, 4, 8, 16, and 24 hours. Then, the mice were sacrificed by cervical dislocation, and the lungs were collected and weighed. Each lung was flushed with distilled water and then homogenised using a homogeniser with 3 mL of PBS and then centrifuged at a speed of 12 000 rpm for 30 minutes; the supernatant was kept in the refrigerator at −80 °C for later analysis.

For the quantification of DOX and TQ, 75 μL of diluted perchloric acid solution, in a ratio of 1.195 to 100 mL distilled water, was added to 300 μL of the supernatant to destroy any remaining lung tissue and centrifuged for 10 min at a speed of 12 000 rpm and then the sample was diluted with 0.5 mL of acetonitrile. The sample was filtered and injected in the HPLC using the same procedure as for TQ and DOX validation.[57]

2.6.3 Toxicity study (protein carbonyl content). In this study, 24 Swiss albino male mice were used with an average weight of 25–30 g. The mice were randomly divided into four groups (n = 6) as shown in Table 1. In this study, the short-term model was used with 2.5 mg kg^{-1} of DOX every other day, six times intraperitoneally.[58,59]

On day 13, the mice were sacrificed by cervical dislocation, and the hearts, livers, and kidneys were collected, flushed with PSB, weighed, and kept in the refrigerator at – 80 °C. After that, the hearts, livers, and kidneys were thawed in an ice bath before being washed in distilled water, cut into small pieces, and ground with a mortar and pestle with liquid nitrogen; the powder was then stored at −80 °C in Eppendorf tubes for later analysis. Using a homogeniser, 50 mg of each sample was homogenised with 1.5 mL of PSB (pH 7.4) with 1% DTT. The homogenate samples were centrifuged at 12 000 rpm at 4 °C for 20 minutes; the supernatant was collected and stored at – 80 °C until needed. To determine the amount of extracted soluble

Table 1 Animal grouping for toxicity study

Groups	Description
Group 1: control group	Untreated mice
Group 2: negative control	Each mouse got 2.5 mg kg^{-1} DOX intraperitoneally every other day for 12 days (total doses = 6)
Group 3: TQ-DOX/Cys-Py/PA NCs	Each mouse got 17 mg of the formula, which contained 2.5 mg of DOX and 9 mg of TQ *via* the inhalation route every other day for 12 days (total doses = 6)
Group 4: DOX/Cys-Py/PA NCs	Each mouse got 19 mg of the DOX polyamide formula, which contained 2.5 mg of DOX, *via* the inhalation route every other day for 12 days (total doses = 6)

proteins present in the samples by the Bradford Assay, 5 μL was taken from each sample and transferred into 96 well plates, and the reading was taken at 595 nm. A bovine serum albumin calibration curve was used.[60] This study used a protein carbonyl content kit from Abcam, UK. According to the kit booklet, the samples were treated with streptozocin to remove the nucleic acid and then DNPH and trichloroacetic acid were added and washed with cold acetone twice to get rid of free DNPH, and then the proteins were solubilised using guanidine solution. After that, 100 μl of each sample was transferred to the 96-well plate, and the absorbance was measured at 375 nm in a microplate reader. The carbonyl content was calculated. The data are presented as mean ± SD. Statistical significance was determined using one-way ANOVA.[61–64]

3. Results and discussion

3.1 Synthesis of polyamide and polyamide loaded with anticancer drugs

3.1.1 Synthesis of L-cystine based polyamide (Cys-Py/PA). Nonpeptidic polyamides were produced using cystine amino acid that acted as a diamine to react with 2,6-pyridine dicarboxylic acid acyl chloride, as shown in Fig. 1. The polycondensation reaction occurred at the interface between the aqueous and organic solutions when cystine in water and acyl dichloride in chloroform were mixed and aggressively agitated. This resulted in the creation of amide bonds. The nucleophilic acyl substitution occurs when the carbonyl carbon atom of 2,6 pyridine dicarboxylic acid acyl chloride reacts with the amino group of cystine amino acid. The diamine reacts with the diacyl chloride at the interface between the two phases. During this reaction, one end of the amine group combines with one end of the diacyl chloride group, forming an amide bond. This amide bond contains two reactive sites, one on each molecule. Subsequently, the amide group elongates to create a lengthy chain of amide bonds.[41–43]

3.1.2 Synthesis of L-cystine based polyamide loaded with TQ and DOX (TQ-DOX/Cys-Py/PA NCs). Interfacial polycondensation is a direct technique in which very reactive monomers are combined in two liquids that do not interact with one another. This method allows for the creation of a polyamide membrane that resembles a capsule.[2] The TQ-DOX/Cys-Py/PA NCs were produced using interfacial polycondensation with 200 mg of TQ added to the chloroform solution and 25 mg of DOX added to the aqueous solution, as shown in Fig. 2. The reaction takes place at the boundary between the liquids,

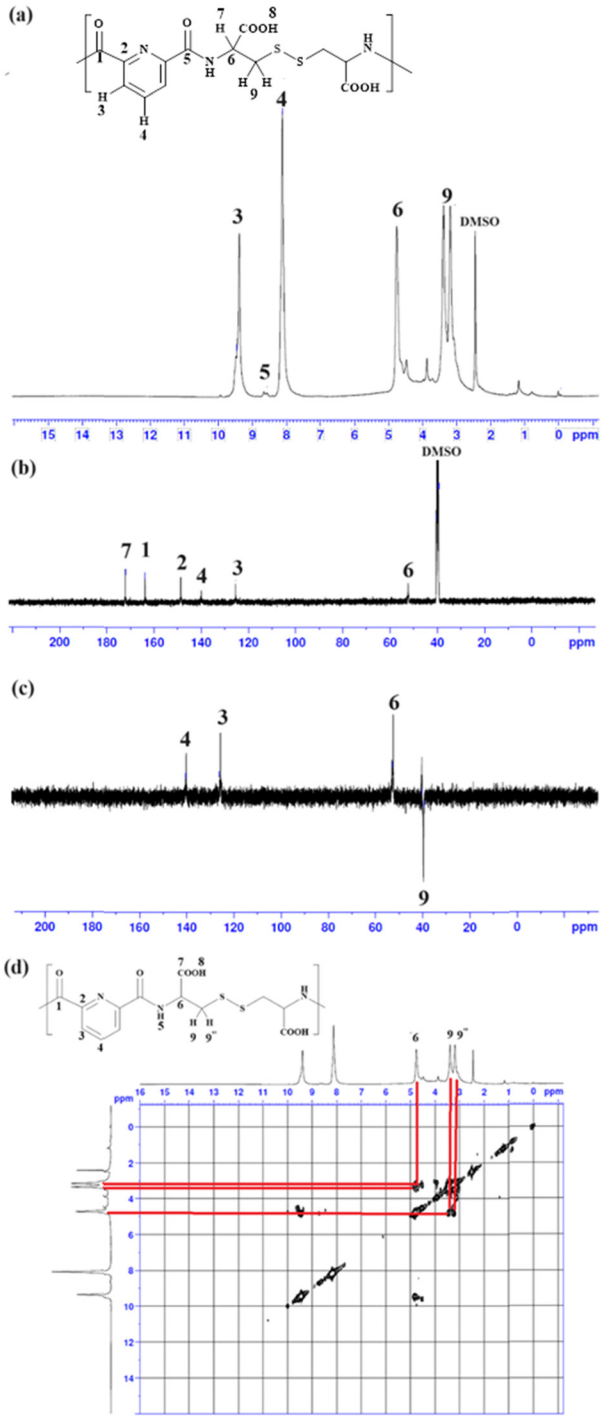

Fig. 1 Synthesis of L-cystine-based polyamide (Cys-Py/PA).

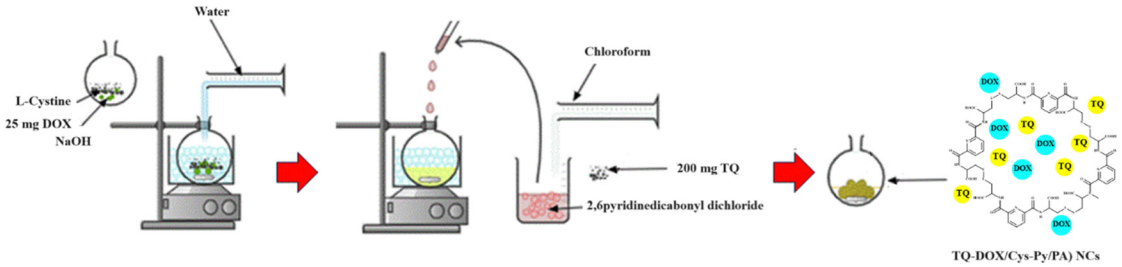

Fig. 2 Synthesis of TQ-DOX/Cys-Py/PA NCs.

leading to the creation of a polymeric shell that surrounds the core solvent. It is a chemical technique used for encapsulation known for its great effectiveness, ability to select the polymer's structure and control over the size of the particles.[42–44]

3.2 Quantification of TQ and DOX using HPLC

According to the ICH requirements for analytical technique validation, the HPLC method for TQ and DOX quantification has been validated.[56] Both actives demonstrated a good linearity over the specified concentration range where the retention time for DOX was 2.46 ± 0.17 min at 550 nm, while TQ eluted at 6.05 ± 0.22 min at 250 nm. The linear calibration curves were created at concentrations that ranged from 3.9 to 62.5 μg mL^{-1} for TQ and from 2.0 to 125 μg mL^{-1} for DOX. Recovery calculations were conducted with percentage recovery ranging from 98.23 to 99.78%. The RSD for the active (TQ and DOX) for all concentrations over three days (9 samples) was less than 2%, indicating that the technique was accurate and precise. The calculated LOD was 2.774 μg mL^{-1} for TQ and 0.942 μg mL^{-1} for DOX, whereas the LOQ was 8.408 μg mL^{-1} for TQ and 2.854 μg mL^{-1} for DOX. Overall, the optimised and validated method was demonstrated to be a good and valid method for the quantification of TQ and DOX. The method was specific to DOX and TQ and the polymer did not dissolve in the dissolution or HPLC medium (CH_3CN).

3.3 Characterisation of Cys-Py/PA and TQ-DOX/Cys-Py/PA NCs

3.3.1 Solubility test. The Cys-Py/PA and TQ-DOX/Cys-Py/PA NCs were insoluble in water. This will have no effect on the polymer used in drug delivery and is often considered a critical factor; it is not the sole determinant of a polymer's effectiveness. Instead, the ability of a polymer to biodegrade into soluble components within the body is of the highest importance. Polymers with peptide amide bonds and disulfide linkages exhibit unique characteristics that facilitate their degradation. The hydrolytic stability of amide groups allows for controlled degradation, while disulfide bonds offer a pathway for redox reactions.

The solubility of the TQ, DOX, Cys-Py/PA, and TQ-DOX/Cys-Py/PA NCs was studied in various common organic solvents; the results are shown in Table 2. Apparently, Cys-Py/PA and TQ-DOX/Cys-Py/PA NCs were soluble in DMSO and slightly soluble in DMF. As both TQ and DOX were soluble in acetonitrile (CH_3CN), they were used for the HPLC standard solutions and calibration curve preparation. The change in the solubility of DOX and TQ in the formula due to the polymer chain surrounding the encapsulated sample (DOX and TQ) changes the solubility upon encapsulation through reduced interaction with solvent molecules.

Table 2 Solubility test for Cys-PA, TQ-DOX PA, TQ and DOX. (+) soluble at room temperature, (–) insoluble at room temperature, and (±) slightly soluble at room temperature

	H_2O	MeOH	EtOH	DMSO	Acetone	$CHCl_3$	DMF	CH_3CN
TQ	–	+	+	+	+	+	+	+
DOX	+	±	+	+	–	–	+	+
Cys-Py/PA	–	–	–	+	–	–	±	–
(TQ-DOX/Cys-P/PA) NCs	–	–	–	+	–	–	±	–

3.3.2 Entrapment efficiency (EE%) and drug loading capacity (DLC%). The EE% and DLC% of TQ and DOX in TQ-DOX/Cys-Py/PA NCs were determined using eqn (1) and (2) respectively. The results showed that the %EE values of TQ and DOX in TQ-DOX/Cys-Py/PA NCs were 85.4% and 99.49% respectively, highlighting high entrapment efficiency and hence an effective process. The DLC% was 52.2% for TQ and 15.03% for DOX.

3.3.3 FTIR analysis. FTIR spectroscopy was used to characterise TQ, DOX, Cys-Py/PA, and TQ-DOX/Cys-Py/PA NCs. The FTIR spectra in Fig. 3 exhibited characteristic absorption bands for all organic functional groups. The FTIR spectrum of TQ exhibited a distinct peak at 2915 cm^{-1}, indicating the stretching of the CH bonds. The presence of a supplementary peak at 1718 cm^{-1} can be attributed to the stretching vibration of the carbonyl (C═O) group in the ketone, as shown in Fig. 3(a). The FTIR spectrum of DOX revealed a characteristic sharp peak at 1730 cm^{-1}, which is attributed to the carbonyl (C═O) group. Additionally, IR bands corresponding to the N–H bond in the amine group were detected at 3320 cm^{-1} and those corresponding to the O–H groups were detected at 3526 cm^{-1}, as shown in Fig. 3(b).[55,65]

The FTIR spectra of Cys-Py/PA and TQ-DOX/Cys-Py/PA NCs exhibited identical characteristic features, which could be attributed to the overlapping of the spectra of Cys-Py/PA and drugs (TQ and DOX). The most important bands exhibit two distinct infrared stretching absorptions that are characteristic of carboxylic acid. The O–H group exhibited a broad spectral range between 2384 and 3648 cm^{-1}, while the C═O group displayed stretching vibrations at 1722 cm^{-1}. Conversely, in the

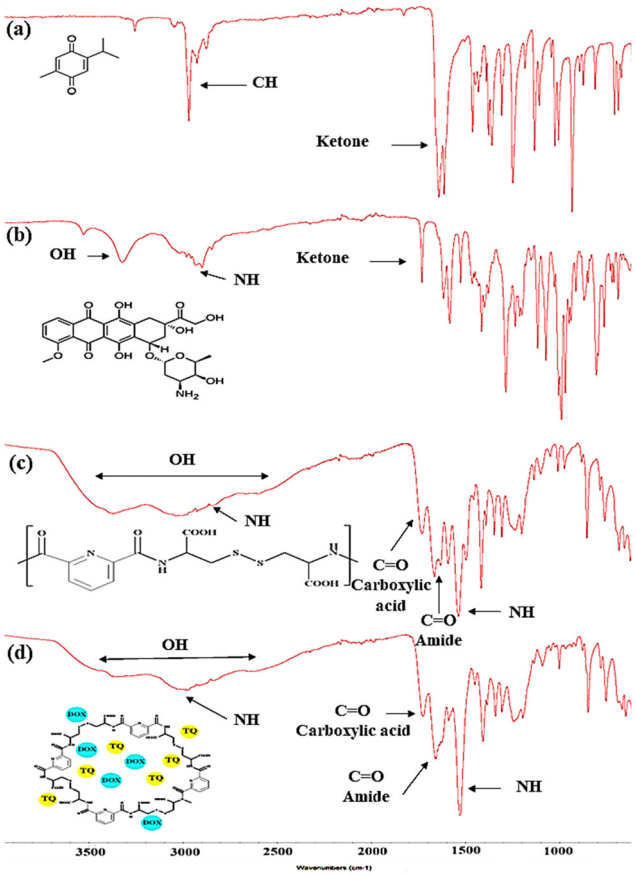

Fig. 3 FTIR spectra of (a) TQ, (b) DOX, (c) Cys-Py/PA, and (d) TQ-DOX/Cys-Py/PA NCs.

amide group, a distinct stretching vibration band for the C═O bond of the formed amide group was observed at approximately 1655 cm^{-1}. Additionally, IR bands corresponding to the N–H bond were detected at 3363 cm^{-1} for stretching vibrations and at 1622 cm^{-1} for bending vibrations, as depicted in Fig. 3(c) and (d).[25]

3.3.4 NMR analysis. The ^{1}H-NMR spectrum of Cys-Py/PA: the proton attached to the carbon atom in the cystine unit was detected at a chemical shift of 4.75 ppm. The CH_2 protons were detected at chemical shifts of 3.38 and 3.18 ppm. The NH proton was detected as a doublet peak at 8.63 ppm. The proton peaks of the pyridine aromatic ring were detected as a duplet peak at 9.42 and 8.11 ppm, as presented in Fig. 4(a).

The ^{13}C-NMR spectrum of Cys-Py/PA: the carbonyl carbon of the amide bond is observed at a chemical shift of 163.85 ppm, while the carbon of the carboxylic acid was observed at a chemical shift of 172.8 ppm. The chemical shifts of the carbons of the pyridine ring unit (CHs) were observed at 139.97 and 125.44, while the quaternary carbon of aromatic pyridine ring carbon was observed at 148.62 ppm. The carbon chemical shift of the CH group attached to the C═O group of the carboxylic acid in Cys-Py/PA was determined at 52.27 ppm. The chemical shift of the carbon in CH_2 was determined at 39.57 ppm, as presented in Fig. 4(b) and (c).

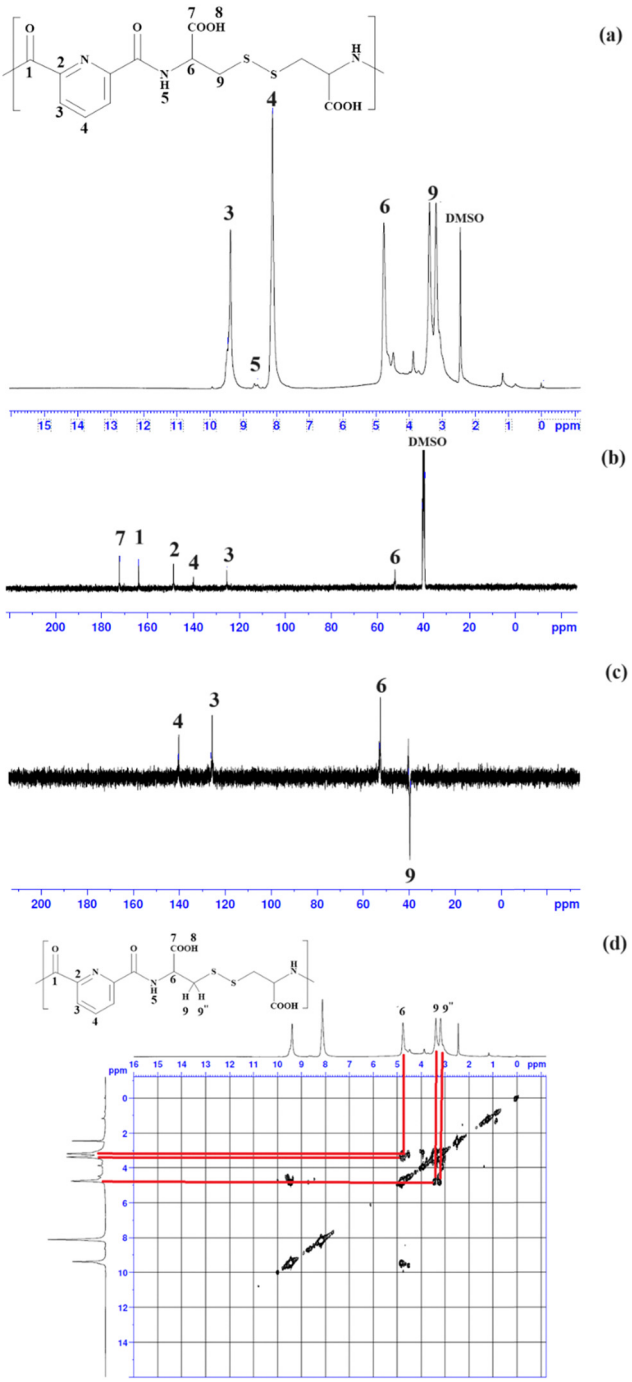

Fig. 4 (a) ^{1}H-NMR, (b) ^{13}C-NMR, (c) DEPT-135, and (d) ^{1}H–^{1}H COSY NMR spectra of Cys-Py/PA.

The 2D-NMR spectrum of Cys-Py/PA: the ^{1}H–^{1}H COSY spectrum indicates the presence of an AMX splitting pattern in the protons of the CH–CH_2 group within the cystine unit. The A, M, and X signals are observed as a pattern consisting of two sets of distinct peaks. Correlations can be observed between the signals of protons labelled as H9 and H9″ and the signal of protons labelled as H6.[66] as shown in the ^{1}H–^{1}H COSY NMR spectrum in Fig. 4(d).

3.3.5 DSC and TGA analyses. Differential scanning calorimetry analysis demonstrated the thermal behaviour of

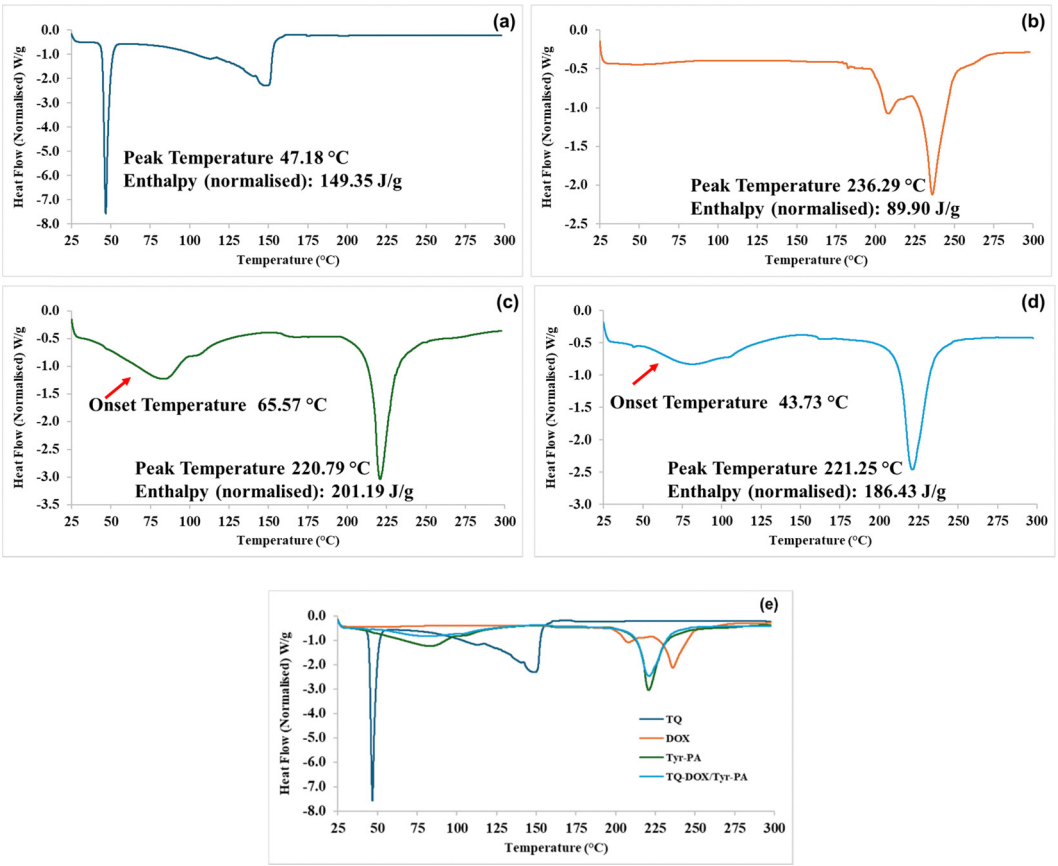

Fig. 5 DSC thermograms of (a) TQ, (b) DOX, (c) Cys-Py/PA, and (d) TQ-DOX/Cys-Py/PA NCs, and (e) compiled thermograms of all the materials.

the used materials. Fig. 5(a) shows the DSC thermograms of TQ, which demonstrated a sharp and well-defined endothermic peak at 47.18 °C with an enthalpy that exceeded 149 J g^{-1}, representing the melting point of TQ and the crystalline nature of the material. The thermogram also reveals another broad endothermic peak at 148.84 °C, corresponding to the decomposition process. The results are in accordance with the findings reported in ref. 67. The thermogram of DOX (Fig. 5(b)) shows an endothermic peak of DOX at 236.29 °C, corresponding to the melting point as reported earlier.[68,69] As for Cys-Py/PA, Fig. 5(c) shows the first endothermic trough that started at the glass transition of the polymer followed by a sharp endothermic peak at 220.79 °C, indicating the semi-crystalline nature of the polymer. The DSC thermogram of the TQ-DOX/Cyd-Py/PA NCs showed a similar trend to the polymer alone, with a wider trough that started earlier (43.73 °C) (Fig. 5(d)), which could be attributed to the interaction of the two actives within the polymeric material.[70] The peaks that represent TQ or DOX melting were not evident from the thermogram of the API (TQ-DOX/Cys-Py/PA NCs), which could be attributed to low content and the encapsulation within the polymeric chain.[65]

The TGA of Cys-Py/PA and the TQ-DOX/Cys-Py/PA NCs is presented in Fig. 6(a) and (b) respectively. The two materials had a moisture content of 3% and the degradation of the polymer started at around 200 °C. From the figures, it could be concluded that the polymer is thermally stable and the addition of the two APIs (TQ and DOX) did not alter the thermal stability of the polymer.

3.3.6 Particle size, zeta potential and TEM analyses. The utilization of nanoscale capsules in pulmonary drug delivery *via* dry powder formulations shows significant advantages, including improved absorption, enhanced solubility, and targeted delivery. The integration of nanoscale capsules in pulmonary drug delivery systems represents a promising frontier in respiratory therapeutics.

Particle size analysis using a Zetasizer indicates the NC size of the Cys-Py/PA and TQ-DOX/Cys-Py/PA NCs, as depicted in Table 3. From the table, it is noted that the Cys-Py/PA and TQ-DOX/Cys-Py/PA NCs are within the nanosize range. A slight increase in the particle size was noted with the addition of the drug due to the encapsulation effect and the increase in size with the encapsulation of the drug within the polymeric chains.[57,71] The particles demonstrated a PDI that ranges between 0.41 and 0.65, indicating the aggregated nature of the Cys-Py/PA and TQ-DOX/Cys-Py/PA NCs.

The TEM micrographs of the TQ-DOX/Cys-Py/PA NCs are presented in Fig. 7. As can be seen, the particles were within the nanosized range. Using Image J software, the average particle size was 19.89 ± 6.5 nm (n = 25). Particles were spherical in shape. However, the average particle size, as obtained from laser diffraction, was 145.99 ± 56.12 nm. This difference in size

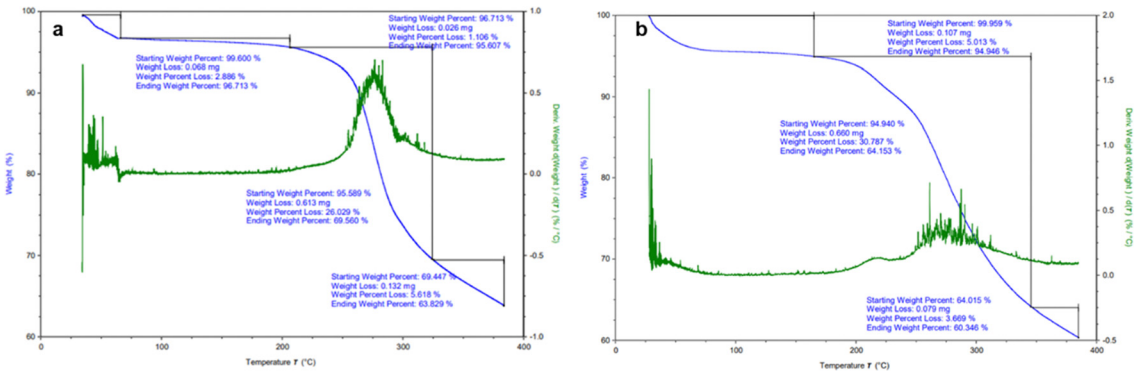

Fig. 6 TGA thermograms of (a) Cys-Py/PA and (b) TQ-DOX/Cys-Py/PA NCs.

Table 3 PSA, PDI, and zeta potential analyses (mean ± SD, n = 3)

Material	Particle size (nm)	Polydispersity index (PDI)	Zeta potential (mV)
TQ	676.5 ± 121.62	0.64 ± 0.21	−4.21 ± 1.57
DOX	518.7 ± 80.76	0.55 ± 0.1	4.94 ± 2.05
Cys-Py/PA	114.9 ± 47.09	0.41 ± 0.03	−30.27 ± 1.01
(TQ/Cys-Py/PA) NCs	125.7 ± 30.76	0.58 ± 0.1	−26.81 ± 0.67
(DOX/Cys-Py/PA) NCs	130.9 ± 57.09	0.48 ± 0.13	−21.83 ± 1.69
(TQ-DOX/Cys-Py/PA) NCs	145.99 ± 56.12	0.65 ± 0.08	−28.30 ± 0.78

using the two methods could be attributed to the nature of the polymeric material. The variance between the particle sizes observed by these two methods was because the TQ-DOX/Cys-Py/PA NCs were swelled with water during DLS. When the TQ-DOX/Cys-Py/PA NCs are subjected to DLS, they come into contact with water, which leads to significant swelling. This polymeric type exhibits a remarkable swelling capacity of approximately 200% within 20 minutes. As the NCs absorb water, their dimensions expand, resulting in a larger apparent size when measured by DLS. This swelling highlights the influence of hydration on the physical characteristics of nanoparticles, necessitating careful interpretation of DLS results.[25,71] In contrast, TEM showed the definite size of the NCs. Such phenomena were previously reported, where using laser diffraction analysis, it was found that the presence of a hydrodynamic layer around the polymeric material could affect the size, and, hence, a larger particle size was observed.[5] Furthermore, the NCs aggregated with a PDI exceeding 0.41 during the laser diffraction analysis; therefore, the presence of aggregates added to the discrepancy in the particle size. The zeta potential of the produced polymeric NCs (CYS-PA) was on the negative scale (−30.27 ± 1.01 mV). Such results are promising as they can aid colloidal de-aggregation of the particles due to repulsive forces between particles. However, the charge was reduced upon encapsulation of the two actives due to the neutral charge of the actives.

3.3.7 XRD analysis. X-Ray diffraction analysis of Cys-Py/PA and TQ-DOX/Cys-Py/PA NCs is depicted in Fig. 8. The XRD patterns of the Cys-Py/PA and TQ-DOX/Cys-Py/PA NCs revealed the semicrystalline nature of the polymer. The XRD patterns of Cys-Py/PA revealed some features of crystallinity with characteristic peaks at 19.85°, 21.7°, 32.5°, and 46.6°. The same peaks were evident for the TQ-DOX/Cys-Py/PA NCs. However, TQ-DOX/Cys-Py/PA NCs did not reveal any additional peaks that are related to the APIs (TQ and DOX). This could be attributed to the low content of TQ and DOX within the polymer and the encapsulation effect.

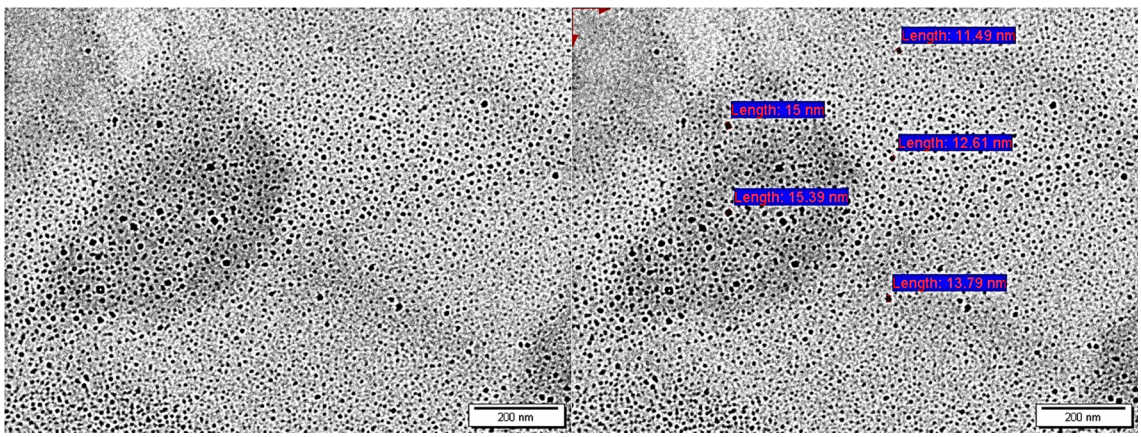

Fig. 7 TEM micrographs of TQ-DOX/Cys-Py/PA NCs highlighting the particle shape and size. Scale bar = 200 nm.

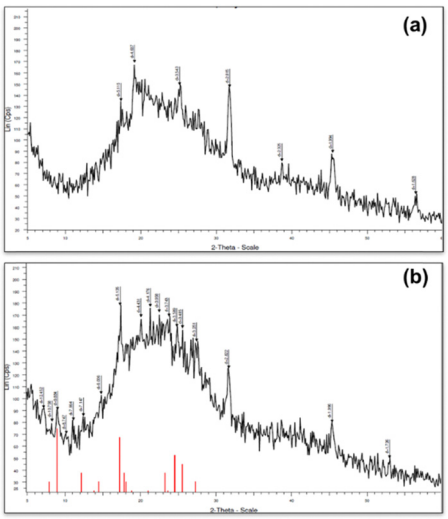

Fig. 8 Powder XRD patterns: (a) Cys-Py/PA and (b) TQ-DOX/Cys-Py/PA NCs.

3.4 *In vitro* study

3.4.1 *In vitro* assessment of the aerodynamic dispersion of the NCs. The NGI study was tasked with assessing the aerodynamic dispersion of NCs loaded with TQ and DOX. The results are summarised in Fig. 9(a), which includes the evaluation of %ED, %FPF_{ED}, RD, and FPF_{TD}. The ED refers to the percentage of the nominated dose that is released from the capsules upon actuation.[72] The results indicated that the prepared TQ-DOX/Cys-Py/PA NCs were able to deliver 98.7% and 97.9% of the nominated dose (7000 μg per puff for TQ and 2000 μg per puff for DOX, respectively). RD, which represents the amount of the API that reached the lower respiratory system, showed high quantities for both actives. FPF_{ED} represents the percentage of the emitted dose that can reach the lower parts of the respiratory system and the aerodynamic particle size was between 1 and 5 μm.[2,67] The FPF_{ED} for TQ and DOX released from the produced TQ-DOX/Cys-Py/PA NCs was 54.3% and 56.3%, respectively. FPF_{TD} represents the percentage of the theoretical dose that is within the range of 1–5 μm and that will reach the lower respiratory system parts.

In general, the aerodynamic performance results of the synthesised NC formulations containing TQ and DOX highlighted the nano-aggregates' capability and efficiency in delivering particles to the lungs. The low SD of the aerodynamic parameters indicated the reproducibility of results in Fig. 9(b).

3.4.2 Release study. Cancer cells often have altered glutathione metabolism, helping them survive oxidative stress and resist chemotherapy. Glutathione-responsive drug delivery systems, usually biodegradable polymers, are designed to release drugs in response to high glutathione levels in cancer cells. These systems use disulfide linkages that are cleaved by glutathione, releasing the drug specifically in tumor cells. This selective release enhances drug effectiveness while reducing

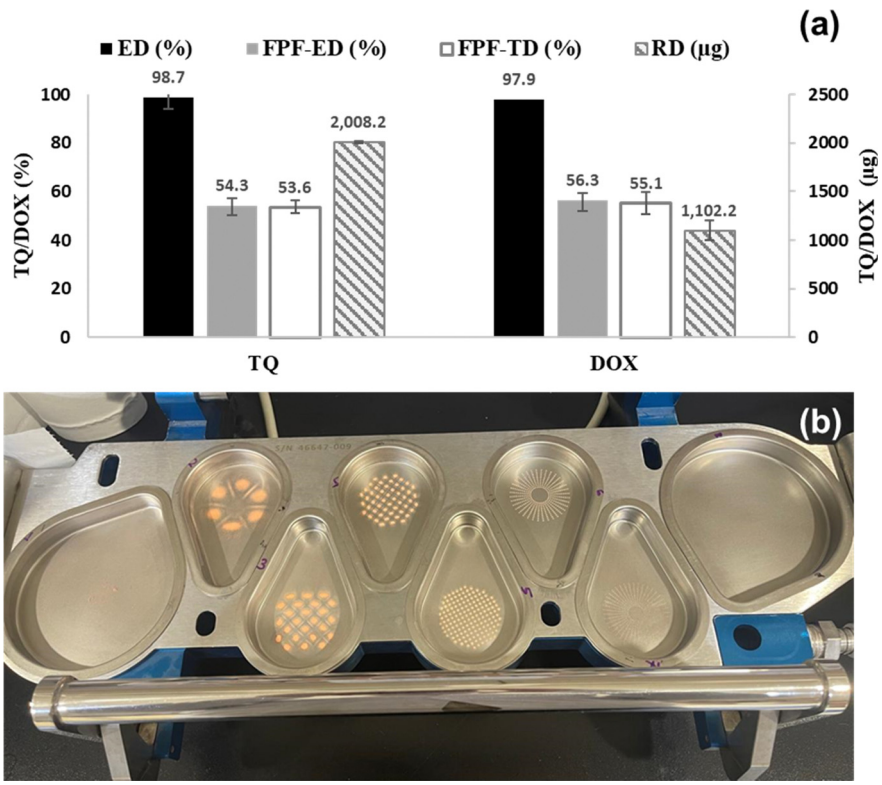

Fig. 9 (a) Aerodynamic dispersion parameters of TQ and DOX from TQ-DOX/Cys-Py/PA NCs; ED: emitted dose; FPF-ED: fine particle fraction of emitted dose; FPF-TD: fine particle fraction of theoretical dose; and RD: respirable dose. Results are presented as mean ± SD, n = 3 and (b) the deposition of the TQ and DOX aggregates of TQ-DOX/Cys-Py/PA NCs onto the NGI trays as orange powder from tray 1 to tray 7.

side effects in healthy tissues. By exploiting elevated glutathione in cancer cells, these systems offer targeted, more precise cancer therapies, improving treatment efficacy and safety.[73,74] In this work a disulfide containing polymer was made and the *in vitro* release was investigated with and without glutathione.

TQ and DOX behaviours were investigated in PBS with a pH of 7.4, at 37 °C, in the presence or absence of GSH. Fig. 10 shows the release patterns of TQ and DOX as time progresses. The release profile of DOX from 0.1 M GSH-containing buffer solution demonstrated a faster onset of action, with 50% released within the first 2 hours. This would be favourable, as once the nanoparticles are taken up by the cancer cell that contains higher GSH levels, the drug will be immediately released. However, when GSH was not added, there was a delay in release for almost 6 hours to start releasing the drug from NCs. Overall, after 24 hours, the release in the two media reached almost 80%. As for TQ, similar to DOX, the 0.1 M GSH containing media promoted the degradation of the polymer and hence faster release of the drug with 50% release within the first 2 hours.[55,75]

3.5 *In vivo* study

3.5.1 *In vivo* aerodynamic performance study. Aerodynamic performance analysis is a critical step in understanding the behaviour and mechanism of TQ-DOX/Cys-Py/PA NC release and deposition at the site of action.[76] Results of the animal study for TQ and DOX deposition in the lungs are presented in Fig. 11(a) and (b), respectively. The present study's finding revealed that inhaled treatment with TQ-DOX/Cys-Py/PA NCs could deliver TQ and DOX directly to the lungs and achieve a sustained release of TQ and DOX in the lungs for at least 24 hours after the treatment. The lung deposition within the first 24 h was 0.4% for TQ and 40% DOX.

NCs are promising drug delivery systems with numerous biological benefits *in vivo*.[77] These tiny molecules can quickly penetrate physiological barriers and reach target locations with high drug concentrations.[78] Natural NCs are biocompatible and biodegradable and have lower side effects than alternative drug delivery systems.[79,80] The use of inhalable natural NCs provides significant advantages in medical treatment by enhancing targeted therapy and reducing systemic toxicity. These NCs are designed to deliver drugs directly to the lung, allowing for more precise targeting of respiratory diseases. This targeted approach ensures that the medication reaches the affected area more efficiently, improving therapeutic outcomes. Additionally, by localising the drug delivery, systemic exposure to the medication is minimised, which significantly reduces the risk of side effects and systemic toxicity. This method not only improves the efficacy of the treatment but also enhances patient safety and comfort.[81,82] In this regard, this study was undertaken with the assumption that employing NCs *via* inhalation can be an effective and safe approach to improving delivery of TQ and DOX drugs. The study found that inhaling NCs delivered TQ and DOX directly to the lung, resulting in sustained increases in TQ and DOX lung concentration after 0.5, 1, 2, 4, 8,16, and 24 hours of therapy (see Fig. 11). These findings suggest that TQ and DOX can directly reach the lung without passing through the gastrointestinal tract or liver. These findings indicate that inhaling NCs can provide a rapid therapeutic response while

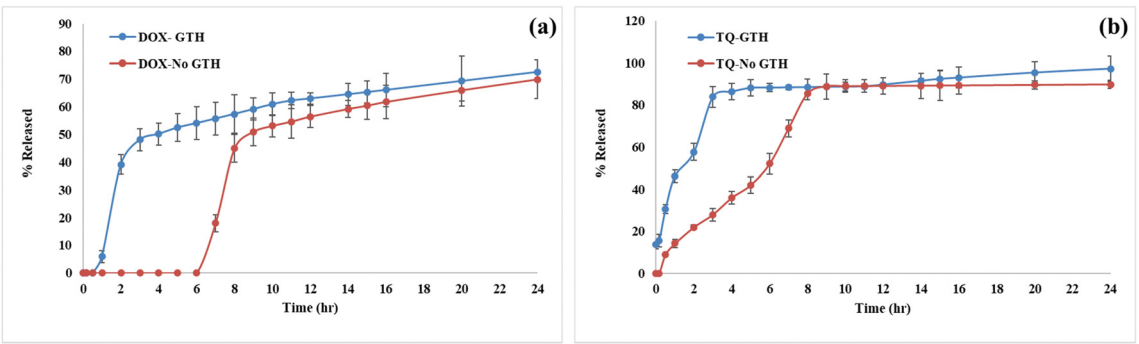

Fig. 10 DOX and TQ release profiles in phosphate buffer (pH = 7.4), with and without glutathione (GSH), (mean ± SD, n = 3).

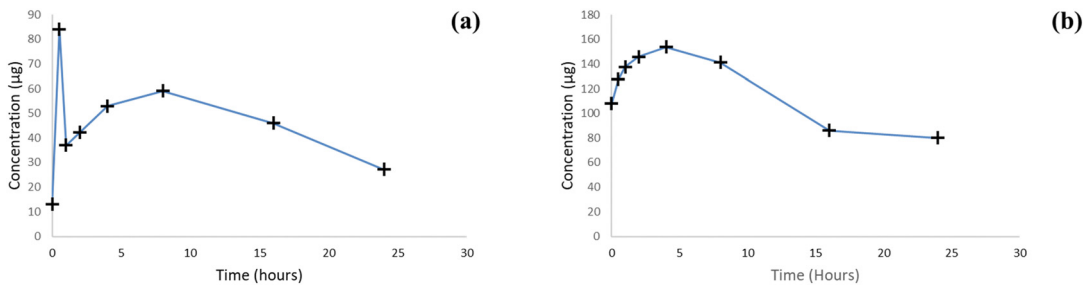

Fig. 11 The concentration–time curve of (a) TQ and (b) DOX in mouse lungs.

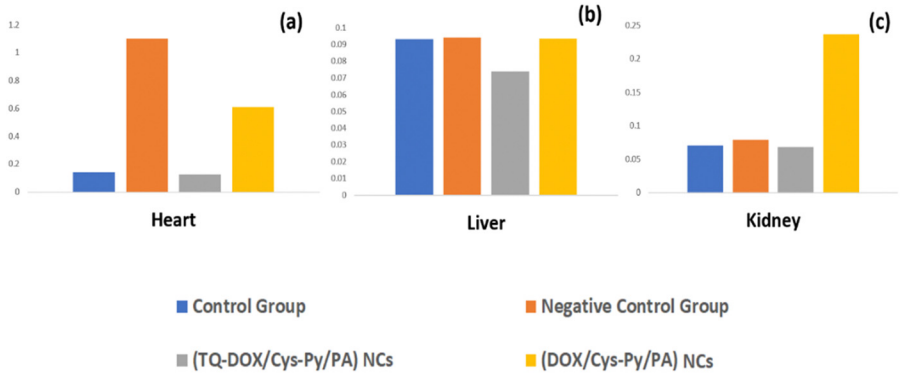

Fig. 12 Protein carbon content in the (a) heart, (b) liver, and (c) kidney.

avoiding the adverse effects of oral DOX treatment. However, additional pharmacological studies are needed to corroborate these findings.

3.5.2 Toxicity study (protein carbonyl content). Carbonyl content is a common marker of oxidative stress and measures oxidative damage. The oxidation of proteins results in the production of stable carbonyl groups, which can be used to measure oxidative injury.[60,83] These modifications modify the structures and functions of proteins, resulting in changes in their biological functions.[84] The findings of the current study showed that at $p < 0.05$, mice in group 2 exhibited a significant difference in the heart protein carbonyl content compared with group 1 ($p = 0.00024$), which may be due to the rise in oxidative stress and cardiotoxicity resulting from the DOX side effect, and showed no significant difference compared with group 4 ($p = 0.06812$); this indicates that the prepared DOX/Cys-Py/PA may play a role in cardiotoxicity related to the DOX side effect. In contrast, it showed a significant increase in protein carbonyl content compared with group 3 ($p = 0.00020$); this may indicate that the prepared TQ-DOX/Cys-Py/PA NCs had reduced the cardiotoxicity side effect resulting from DOX, in addition to the antioxidant effect of TQ, which also helps in attenuating the cardiotoxicity resulting from DOX Fig. 12(a). These results are consistent with previous studies showing the toxicity of DOX to the heart,[37,85] and studies show the role of TQ in reducing this toxicity.[86]

At the liver level, there was no significant increase in the carbonyl content; this indicates that no liver injury happened to the treated mice in the 4 groups ($p = 0.336862$), Fig. 12(b); this may be due to the low dose of DOX since the previous literature found that the low dose of DOX does not cause liver toxicity.[87]

In kidneys, a significant increase in carbonyl content in group 4 was observed compared with the other groups ($p < 0.00001$), and this may indicate that the prepared Cys-Py/PA may cause an increase in oxidative stress in the kidney; on the other hand, the mice in group 3 showed no significant difference compared to those in groups 1 and 2 ($p = 0.99743$ and 0.79346), respectively, and this may be due to the antioxidant effect of TQ on reducing the nephrotoxicity (Fig. 12(c)). However, additional pharmacological studies are needed to corroborate these findings.

4. Conclusions

Developing dry powder inhalers (DPIs) that have a consistent distribution of ingredients and consistent ability to reach the desired areas of the respiratory system is difficult. Hence, the objective of this project was to create a fixed-dose combination (FDC) of TQ and DOX. Using an interfacial polycondensation method, this combination was loaded onto a new cystine-based polyamide. The process involved polymerisation and encapsulation of TQ and DOX, all done in a single step. The aerodynamic performance assessment showed that the formulated substance could deliver 98.7% and 97.1% of the intended dose to the lungs. The emitted dose could reach the lower regions of the respiratory system effectively. The particle size ranges from 1 to 5 μm, which makes it well-suited for aerodynamic purposes. In addition, when examined in a 0.1 M GSH-containing buffer solution, TQ and DOX were selectively released, demonstrating a swift initiation of activity, with 50% of the compounds being released within the first 2 hours. *In vivo* studies showed that the formula enables targeted drug delivery to treat lung cancer. Toxicity was assessed by measuring protein carbonyl content. The prepared TQ-DOX/Cys-Py/PA NCs had lower heart, liver, and kidney toxicity. Overall, this study developed and applied novel TQ and DOX NCs to deliver anticancer drugs to the lung through pulmonary administration. This treatment can exert its effects specifically in the localised area of lung cancer.

Author contributions

Hadeel Hafez Banat: writing – original draft, methodology, investigation, formal analysis and data curation; Dalia Khalil Ali: writing – original draft, writing – reviewing, editing the final version of the draft, project conceptualization and administration, methodology, formal analysis, funding acquisition; Qais Jarrar: methodology, formal analysis, data curation, writing – original draft, writing – reviewing and editing; Esra'a Alomary: methodology, data curation; and Eman Zmaily Dahmash: writing – original draft, writing – reviewing, editing the final version of the draft, project conceptualization, methodology, formal analysis.

Data availability

All the data used in this research project are included in the study.

Conflicts of interest

The authors confirm that there are no conflicts to declare.

Acknowledgements

The authors acknowledge the support of Isra University (Jordan) for funding Dr Dalia Ali (4-18/2022/2023). Also, the authors further acknowledge Kingston University for supporting Dr Eman Dahmash.

References

1 R. Wen, A. C. Umeano, P. Chen and A. A. Farooqi, Polymer-based drug delivery systems for cancer, *Crit. Rev. Ther. Drug Carrier Syst.*, 2018, **35**(6), 521–554, DOI: **10.1615/CritRevTherDrugCarrierSyst.2018021124**.

2 H. AbdulKarim, D. K. Ali, E. Taybeh, H. S. Alyami, S. M. Assaf and E. Z. Dahmash, Novel poly (ester amide) derived from tyrosine amino acid for targeted pulmonary drug delivery of fluticasone propionate, *J. Appl. Polym. Sci.*, 2023, e53672.

3 N. M. Al-baldawi, D. Khalil, Q. Jarrar, R. Abuthawabeh and E. Zmaily, *Journal of Drug Delivery Science and Technology Quality by design for the synthesis and optimisation of arginine-poly(ester-amide) nanocapsules as promising carriers for nose-brain delivery of carbamazepine*, 89, 2023.

4 M. H. Alyami, E. Z. Dahmash, D. K. Ali, H. S. Alyami, H. AbdulKarim and S. A. Alsudir, Novel Fluticasone Propionate and Salmeterol Fixed-Dose Combination Nano-Encapsulated Particles Using Polyamide Based on L-Lysine, *Pharmaceuticals*, 2022, **15**(3), 321.

5 E. Z. Dahmash, L. M. Attiany, D. Ali, S. M. Assaf, J. Alkrad and H. Alyami, Development and Characterization of Transdermal Patches Using Novel Thymoquinone-L-Arginine-Based Polyamide Nanocapsules for Potential Use in the Management of Psoriasis, *AAPS PharmSciTech*, 2024, **25**(4), 1–16, DOI: **10.1208/s12249-024-02781-2**.

6 J. Kaur, *et al.*, A hand-held apparatus for 'nose-only' exposure of mice to inhalable microparticles as a dry powder inhalation targeting lung and airway macrophages, *Eur. J. Pharm. Sci.*, 2008, **34**(1), 56–65, DOI: **10.1016/j.ejps.2008.02.008**.

7 R. Gobi, P. Ravichandiran, R. S. Babu and D. J. Yoo, Biopolymer and synthetic polymer-based nanocomposites in wound dressing applications: A review, *Polymers*, 2021, **13**(12), 1962, DOI: **10.3390/polym13121962**.

8 M. F. Maitz, Applications of synthetic polymers in clinical medicine, *Biosurf. Biotribol.*, 2015, **1**(3), 161–176, DOI: **10.1016/j.bsbt.2015.08.002**.

9 Z. Liang, R. Ni, J. Zhou and S. Mao, Recent advances in controlled pulmonary drug delivery, *Drug Discovery Today*, 2015, **20**(3), 380–389, DOI: **10.1016/j.drudis.2014.09.020**.

10 F. Lavorini, M. Pistolesi and O. S. Usmani, Recent advances in capsule-based dry powder inhaler technology, *Multidiscip. Respir. Med.*, 2017, **12**(1), 11, DOI: **10.1186/s40248-017-0092-5**.

11 H. Banat, R. Ambrus and I. Csóka, Drug combinations for inhalation: Current products and future development addressing disease control and patient compliance, *Int. J. Pharm.*, 2023, **643**, 123070, DOI: **10.1016/j.ijpharm.2023.123070**.

12 Q. Fei, I. Bentley, S. N. Ghadiali and J. A. Englert, Pulmonary drug delivery for acute respiratory distress syndrome, *Pulm. Pharmacol. Ther.*, 2023, **79**, 102196, DOI: **10.1016/j.pupt.2023.102196**.

13 J. S. Patton, C. S. Fishburn and J. G. Weers, The Lungs as a Portal of Entry for Systemic Drug Delivery, *Proc. Am. Thorac. Soc.*, 2004, **1**(4), 338–344, DOI: **10.1513/pats.200409-049TA**.

14 P. Sharma, *et al.*, Emerging trends in the novel drug delivery approaches for the treatment of lung cancer, *Chem. – Biol. Interact.*, 2019, **309**, 108720, DOI: **10.1016/j.cbi.2019.06.033**.

15 J. S. Patil and S. Sarasija, Pulmonary drug delivery strategies: A concise, systematic review, *Lung India*, 2012, **29**(1), 44–49, DOI: **10.4103/0970-2113.92361**.

16 N. Politakos, V. G. Gregoriou and C. L. Chochos, *Pulmonary Drug Delivery through Responsive Materials*, pp. 490–508, 2024.

17 W. Lee, E. Lee, D. Jang, Y. Cho, J. Cha and H. Lee, Polymeric Carriers for Pulmonary Drug Delivery, *Yakhak Hoeji*, 2016, **60**(4), 173–179, DOI: **10.17480/psk.2016.60.4.173**.

18 Y. Javadzadeh and S. Yaqoubi, Therapeutic nanostructures for pulmonary drug delivery, *Nanostructures for Drug Delivery*, Elsevier, 2017, pp. 619–638.

19 M. Kumar, A. R. Hilles, S. Hamed, A. Bhatia and S. Mahmood, Micro and nano-carriers-based pulmonary drug delivery system: Their current updates, challenges, and limitations – A review, *JCIS Open*, 2023, **12**, 100095, DOI: **10.1016/j.jciso.2023.100095**.

20 S. S. Gupta, V. Mishra, M. Das Mukherjee, P. Saini and K. R. Ranjan, Amino acid derived biopolymers: Recent advances and biomedical applications, *Int. J. Biol. Macromol.*, 2021, **188**, 542–567.

21 W. Lu, X. Wang, R. Cheng, C. Deng, F. Meng and Z. Zhong, Biocompatible and bioreducible micelles fabricated from novel α-amino acid-based poly(disulfide urethane)s: Design, synthesis and triggered doxorubicin release, *Polym. Chem.*, 2015, **6**(33), 6001–6010, DOI: **10.1039/c5py00828j**.

22 M. Pechar, A. Braunová, K. Ulbrich, M. Jelínková and B. Říhová, Poly(ethylene glycol)-doxorubicin conjugates with pH-controlled activation, *J. Bioact. Compat. Polym.*, 2005, **20**(4), 319–341, DOI: **10.1177/0883911505055161**.

23 A. C. Fonseca, M. H. Gil and P. N. Simões, Biodegradable poly(ester amide)s – A remarkable opportunity for the biomedical area: Review on the synthesis, characterization and applications, *Prog. Polym. Sci.*, 2014, **39**(7), 1291–1311, DOI: **10.1016/j.progpolymsci.2013.11.007**.

24 B. Al-tayyem and B. Sweileh, Synthesis, characterization and hydrolytic degradation of novel biodegradable poly(ester amide) s derived from Isosorbide and α-amino acids, *J. Polym. Res.*, 2020, **27**(5), 1–14.
25 D. K. Ali, A. M. Al-Zuheiri and B. A. Sweileh, pH and reduction sensitive bio-based polyamides derived from renewable dicarboxylic acid monomers and cystine amino acid, *Int. J. Polym. Anal. Charact.*, 2017, **22**(4), 361–373, DOI: 10.1080/1023666X.2017.1298012.
26 S. H. S. Boddu, *et al.*, *Polyamide/Poly(Amino Acid) Polymers for Drug Delivery*, 2021.
27 M. Miyamoto, *et al.*, Improved nasal absorption of drugs using poly-l-arginine: effects of concentration and molecular weight of poly-l-arginine on the nasal absorption of fluorescein isothiocyanate–dextran in rats, *Eur. J. Pharm. Biopharm.*, 2001, **52**(1), 21–30, DOI: 10.1016/S0939-6411(01)00149-7.
28 E. Stiegelmaier, T. C. Costa, G. Pakuszewski, S. M. A. Guelli Ulson de Souza, A. A. Ulson de Souza and A. P. Serafini Immich, Enhancing polyamide 6: Acid hydrolysis for functionalization and amino group quantification, *Polymer*, 2024, **298**, 126905, DOI: 10.1016/J.POLYMER.2024.126905.
29 Y. Tao, X. Tan and T. Zhang, Enhancing biocompatibility and degradation control of biodegradable polymers through amino acid grafting: A study on 4arm-PLGA-Amino acid copolymers, *Appl. Mater. Today*, 2024, **41**, 102497, DOI: 10.1016/J.APMT.2024.102497.
30 J. V. González-Aramundiz, M. V. Lozano, A. Sousa-Herves, E. Fernandez-Megia and N. Csaba, Polypeptides and polyaminoacids in drug delivery, *Expert Opin. Drug Delivery*, 2012, **9**(2), 183–201, DOI: 10.1517/17425247.2012.647906.
31 É. A. de Souza, *et al.*, Incorporation of the chemotherapy medication cisplatin into polyamide membrane, *J. Inorg. Biochem.*, 2018, **180**, 171–178, DOI: 10.1016/J.JINORGBIO.2017.12.013.
32 J. Wu, *et al.*, Hydrophobic Cysteine Poly(disulfide)-based Redox-Hypersensitive Nanoparticle Platform for Cancer Theranostics, *Angew. Chem., Int. Ed.*, 54, 32, 9218–9223, 2015, DOI: 10.1002/anie.201503863.
33 L. Yu, L. Kong, J. Xie, W. Wang, C. Chang and H. Che, Reduction-sensitive *N*,*N*′-Bis(acryloyl) cystinamide-polymerized Nanohydrogel as a Potential Nanocarrier for Paclitaxel Delivery, *Des. Monomers Polym.*, 2021, **24**(1), 98–105, DOI: 10.1080/15685551.2021.1914398.
34 N. Traverso, *et al.*, Role of glutathione in cancer progression and chemoresistance, *Oxid. Med. Cell. Longevity*, 2013, **2013**, 972913, DOI: 10.1155/2013/972913.
35 S. P. Hadipour Moghaddam, J. Saikia, M. Yazdimamaghani and H. Ghandehari, Redox-Responsive Polysulfide-Based Biodegradable Organosilica Nanoparticles for Delivery of Bioactive Agents, *ACS Appl. Mater. Interfaces*, 2017, **9**(25), 21133–21146, DOI: 10.1021/acsami.7b04351.
36 J. J. C. Neefjes, *et al.*, *New insights into the activities and toxicities of the old anti-cancer drug doxorubicin*. 2020.
37 H. S. Al-malky, S. E. Al Harthi and A. M. M. Osman, Major obstacles to doxorubicin therapy: Cardiotoxicity and drug resistance, *J. Oncol. Pharm. Pract.*, 2020, **26**(2), 434–444, DOI: 10.1177/1078155219877931.
38 S. Sritharan and N. Sivalingam, Review article A comprehensive review on time-tested anticancer drug doxorubicin, *Life Sci.*, 2021, **278**, 119527, DOI: 10.1016/j.lfs.2021.119527.
39 M. Xu, *et al.*, PEG-Detachable Polymeric Micelles Self-Assembled from Amphiphilic Copolymers for Tumor-Acidity-Triggered Drug Delivery and Controlled Release, *ACS Appl. Mater. Interfaces*, 2019, **11**(6), 5701–5713, DOI: 10.1021/acsami.8b13059.
40 Q. Guo, *et al.*, Doxorubicin-loaded natural daptomycin micelles with enhanced targeting and anti-tumor effect in vivo, *Eur. J. Med. Chem.*, 2021, **222**, 113582, DOI: 10.1016/j.ejmech.2021.113582.
41 I. Micallef and B. Baron, Annals of Clinical Toxicology Doxorubicin: An Overview of the Anti-Cancer and Chemoresistance Mechanisms, 2020.
42 O. Tacar, P. Sriamornsak and C. R. Dass, Doxorubicin: an update on anticancer molecular action, *J. Pharm. Pharmacol.*, 2013, 157–170, DOI: 10.1111/j.2042-7158.2012.01567.x.
43 A. H. Rahmani and S. M. Aly, Nigella Sativa and its active constituents thymoquinone shows pivotal role in the diseases prevention and treatment NIGELLA SATIVA AND ITS ACTIVE CONSTITUENTS THYMOQUINONE SHOWS PIVOTAL, no. January, 2015.
44 A. Ahmad, M. Raish and K. M. Alkharfy, The potential role of thymoquinone in preventing the cardiovascular complications of COVID-19, *Vasc. Pharmacol.*, 2021, 106899, DOI: 10.1016/j.vph.2021.106899.
45 M. A. Khan, M. Tania, S. Fu and J. Fu, Thymoquinone, as an anticancer molecule: From basic research to clinical investigation, *Oncotarget*, 2017, **8**(31), 51907–51919, DOI: 10.18632/oncotarget.17206.
46 S. Slezakova and J. Ruda-Kucerova, Anticancer activity of artemisinin and its derivatives, *Anticancer Res.*, 2017, **37**(11), 5995–6003, DOI: 10.21873/anticanres.12046.
47 K. E. R. Schobert, Combinatorial effects of thymoquinone on the anti-cancer activity of doxorubicin, *Cancer Chemother. Pharmacol.*, 2011, 867–874, DOI: 10.1007/s00280-010-1386-x.
48 F. Abbaspour, M. Mahboubeh, E. Fatemeh and R. Y. Robati, Effect of thymoquinone – loaded lipid – polymer nanoparticles as an oral delivery system on anticancer efficiency of doxorubicin, *J. Nanostruct. Chem.*, 2021, 0123456789, DOI: 10.1007/s40097-021-00398-6.
49 M. Abukhader, Thymoquinone in The clinical Treatment of cancer: Fact or fiction-, *Pharmacogn. Rev.*, 2013, **7**(14), 117–120, DOI: 10.4103/0973-7847.120509.
50 G. M. Ganea, S. O. Fakayode, J. N. Losso, C. F. Van Nostrum, C. M. Sabliov and I. M. Warner, Delivery of phytochemical thymoquinone using molecular micelle modified poly(D,L-lactide-*co*-glycolide) (PLGA) nanoparticles, *Nanotechnology*, 2010, **21**(28), 285104, DOI: 10.1088/0957-4484/21/28/285104.
51 O. Shadyro, A. Sosnovskaya, I. Edimecheva, L. Kireicikova, S. Samovich, B. Dubovik, S. Krasny and D. Tzerkovsk, Anticancer activity of thymoquinone and its combinations with doxorubicin and linseed oil in the treatment of

xenograft tumors Oleg, *Adv. Tradit. Med.*, 2024, DOI: 10.1007/s13596-024-00785-8.

52 K. M. Ibiyeye, N. Nordin, M. Ajat and A. B. Zuki, Ultrastructural Changes and Antitumor Effects of Doxorubicin/Nanoparticles on Breast Cancer, *Front. Oncol.*, 2019, **9**, 1–14, DOI: 10.3389/fonc.2019.00599.

53 N. E. El-ashmawy, E. G. Khedr, E. M. Ebeid, M. L. Salem, E. M. Mosalam and A. A. Zidan, Loading ofdoxorubicin and thymoquinone with F2 gel nanofibers improves the antitumor activity and ameliorates doxorubicin- associated nephrotoxicity Nahla, *Life Sci.*, 2017, **109**, 525–532, DOI: 10.1016/j.lfs.2018.06.008.

54 E. Rahmani, S. A. Ghorbanian, H. Rashedi and M. Navaee, Preparation of a pH-responsive chitosan-montmorillonite-nitrogen-doped carbon quantum dots nanocarrier for attenuating doxorubicin limitations in cancer therapy, *Eng. Life Sci.*, 2022, 634–649, DOI: 10.1002/elsc.202200016.

55 D. K. Ali, S. H. Al-Ali, E. Z. Dahmash, G. Edris and H. S. Alyami, Reduction and pH Dualresponsive Biobased Poly(disulfide-amide) Nanoparticles Using Cystine Amino Acid for Targeting Release of Doxorubicin Anticancer Drug, *J. Polym. Environ.*, 2022, **30**, 4809–4820, DOI: 10.1007/s10924-022-02552-9.

56 ICH, Validation of analytical procedures: Text and methodology Q2(R1), *Int. Conf. Harmon. Tech. Requir. Regist. Pharm. Hum. Use*, vol. 4, 2005.

57 E. Z. Dahmash, *et al.*, Preclinical evaluation of novel synthesised nanoparticles based on tyrosine poly(ester amide) for improved targeted pulmonary delivery, *Sci. Rep.*, 2024, **14**(1), 1–16, DOI: 10.1038/s41598-024-59588-1.

58 E. Y. Podyacheva, E. A. Kushnareva, A. A. Karpov and Y. G. Toropova, Analysis of models of doxorubicin-induced cardiomyopathy in rats and mice. A modern view from the perspective of the pathophysiologist and the clinician, *Front. Pharmacol.*, 2021, **12**, 1–12, DOI: 10.3389/fphar.2021.670479.

59 X. Liu, X. Wang, X. Zhang, Y. Xie, R. Chen and H. Chen, C57BL/6 mice are more appropriate than BALB/C mice in inducing dilated cardiomyopathy with short-term doxorubicin treatment, *Acta Cardiol. Sin.*, 2012, **28**(3), 236–240.

60 S. Bruno, L. Ronda, G. Paredi, S. Bettati and A. Mozzarelli, Protein carbonylation detection methods: A comparison, *Data Brief*, 2018, **19**, 2215–2220, DOI: 10.1016/j.dib.2018.06.088.

61 N. M. Alkurdi, S. H. Hussein-al-ali, A. Albalwi, M. K. Haddad, Y. Aldalahmed and D. K. Ali, Development and Evaluation of a Novel Polymer Drug Delivery System Using Cromolyn-Polyamides-Disulfide using Response Surface Design, vol. 2022, 2022.

62 Z. A. G. Ahmed, *et al.*, Development and Evaluation of Amlodipine-Polymer Nanocomposites Using Response Surface Methodology, *Int. J. Polym. Sci.*, 2022, **2022**, 427400, DOI: 10.1155/2022/3427400.

63 A. D. Mytara, K. Chronaki, V. Nikitakos, C. D. Papaspyrides, K. Beltsios and S. Vouyiouka, *Synthesis of Polyamide-Based Microcapsules via Interfacial Polymerization: Effect of Key Process Parameters*, 2021.

64 L. Ripoll and Y. Clement, Polyamide microparticles containing vitamin C by interfacial polymerization: an approach by design of experimentation, *Cosmetics*, 2016, **3**(4), 38.

65 E. Z. Dahmash, D. K. Ali, H. S. Alyami, H. Abdulkarim, M. H. Alyami and A. H. Aodah, *Novel Thymoquinone Nanoparticles Using Poly(ester amide) Based on L-Arginine-Targeting Pulmonary Drug Delivery*, 2022.

66 D. K. Ali, Synthesis and Characterization of Novel Biobased Ion – Exchange Bisfuran Polyamides Prepared by Interfacial Polycondensation of Bisfuran Diamine Monomer and Sustainable Dicarboxylic Acid Derivatives, *J. Polym. Environ.*, 2022, **30**, 4102–4113, DOI: 10.1007/s10924-022-02496-0.

67 E. Z. Dahmash, D. K. Ali, H. S. Alyami, H. Abdulkarim, M. H. Alyami and A. H. Aodah, Novel Thymoquinone Nanoparticles Using Poly(Ester Amide) Based on L-Arginine-Targeting Pulmonary Drug Delivery, *Polymers*, 2022, **14**(6), 1082, DOI: 10.3390/polym14061082.

68 K. Songsurang, N. Praphairaksit, K. Siraleartmukul and N. Muangsin, Electrospray fabrication of doxorubicin-chitosan-tripolyphosphate nanoparticles for delivery of doxorubicin, *Arch. Pharmacal Res.*, 2011, **34**(4), 583–592.

69 A. Neacşu, Physicochemical investigation of the complexation between γ-cyclodextrin and doxorubicin in solution and in solid state, *Thermochim. Acta*, 2018, **661**, 51–58, DOI: 10.1016/j.tca.2018.01.012.

70 X. Zhao, *et al.*, Codelivery of doxorubicin and curcumin with lipid nanoparticles results in improved efficacy of chemotherapy in liver cancer, *Int. J. Nanomed.*, 2014, **10**, 257–270, DOI: 10.2147/IJN.S73322.

71 F. Alregeb, F. Khalili, B. Sweileh and D. K. Ali, Synthesis and Characterization of Chelating Hyperbranched Polyester Nanoparticles for Cd(II) Ion Removal from Water, *Molecules*, 2022, **27**(12), 3656, DOI: 10.3390/molecules27123656.

72 S. F. A. Tarawneh, *et al.*, Mechanistic Modelling of Targeted Pulmonary Delivery of Dactinomycin Iron Oxide Loaded Nanoparticles for Lung Cancer Therapy, *Pharm. Dev. Technol.*, 2022, 1–35.

73 R. Iyer, *et al.*, Glutathione-responsive biodegradable polyurethane nanoparticles for lung cancer treatment, *J. Controlled Release*, 2020, **321**, 363–371.

74 J. F. Quinn, M. R. Whittaker and T. P. Davis, Glutathione responsive polymers and their application in drug delivery systems, *Polym. Chem.*, 2017, **8**(1), 97–126.

75 S. Yu, J. Ding, C. He, Y. Cao, W. Xu and X. Chen, Disulfide cross-linked polyurethane micelles as a reduction-triggered drug delivery system for cancer therapy, *Adv. Healthcare Mater.*, 2014, **3**(5), 752–760, DOI: 10.1002/adhm.201300308.

76 F. Yamashita and M. Hashida, Pharmacokinetic considerations for targeted drug delivery, *Adv. Drug Delivery Rev.*, 2013, **65**(1), 139–147, DOI: 10.1016/j.addr.2012.11.006.

77 S. Deng, M. R. Gigliobianco, R. Censi and P. Di Martino, Polymeric nanocapsules as nanotechnological alternative for drug delivery system: current status, challenges and opportunities, *Nanomaterials*, 2020, **10**(5), 847.

78 U. Bazylińska, D. Wawr, J. Kulbacka, R. Frąckowiak, B. Cichy and A. Bednarkiewicz, Polymeric nanocapsules with up-converting nanocrystals cargo make ideal fluorescent bio-probes, *Sci. Rep.*, 2016, **6**(1), 29746, DOI: **10.1038/srep29746**.
79 R. T. Branquinho, *et al.*, Biodegradable polymeric nanocapsules prevent cardiotoxicity of anti-trypanosomal lychnopholide, *Sci. Rep.*, 2017, **7**(1), 1–13.
80 Y. Yao, *et al.*, Nanoparticle-Based Drug Delivery in Cancer Therapy and Its Role in Overcoming Drug Resistance, *Front. Mol. Biosci.*, 2020, **7**, 1–14, DOI: **10.3389/fmolb.2020.00193**.
81 W. H. Lee, C. Y. Loo, D. Traini and P. M. Young, Inhalation of nanoparticle-based drug for lung cancer treatment: Advantages and challenges, *Asian J. Pharm. Sci.*, 2015, **10**(6), 481–489, DOI: **10.1016/j.ajps.2015.08.009**.
82 P. Muralidharan, M. Malapit, E. Mallory, D. Hayes and H. M. Mansour, Inhalable nanoparticulate powders for respiratory delivery, *Nanomedicine*, 2015, **11**(5), 1189–1199, DOI: **10.1016/j.nano.2015.01.007**.
83 Y. R. Song, J. Kim, H. Lee, S. G. Kim and E. Choi, *Serum levels of protein carbonyl, a marker of oxidative stress, are associated with overhydration, sarcopenia and mortality in hemodialysis patients*, pp. 1–11, 2020.
84 A. Mitsugu, Protein carbonylation: molecular mechanisms, biological implications, and analytical approaches, *Free Radical Res.*, 2021, **55**(4), 307–320, DOI: **10.1080/10715762.2020.1851027**.
85 Y. K. Kim, *The use of polyolefins in industrial and medical applications*, Elsevier Ltd, 2017.
86 D. Karabulut, E. Ozturk, E. Kaymak, A. T. Akin and B. Yakan, Thymoquinone attenuates doxorubicin-cardiotoxicity in rats, *J. Biochem. Mol. Toxicol.*, 2021, **35**(1), 1–9, DOI: **10.1002/jbt.22618**.
87 K. N. Timm, *et al.*, Metabolic Effects of Doxorubicin on the Rat Liver Assessed With Hyperpolarized MRI and Metabolomics, *Front. Physiol.*, 2022, **12**, 1–8, DOI: **10.3389/fphys.2021.782745**.